

Nanocomposites from styrene–butadiene rubber (SBR) and multiwall carbon nanotubes (MWCNT) part 2: Mechanical properties



S.K. Peddini ^a, C.P. Bosnyak ^b, N.M. Henderson ^b, C.J. Ellison ^{a,*}, D.R. Paul ^a

^a McKetta Department of Chemical Engineering and Texas Materials Institute, The University of Texas at Austin, Austin, TX 78712, USA

^b Molecular Rebar Design, LLC, 13477 Fitzhugh Rd, Austin, TX 78736, USA

ARTICLE INFO

Article history:

Received 24 September 2014

Accepted 2 November 2014

Available online 11 November 2014

Keywords:

Multiwall carbon nanotubes

Crack bridging

Tear energy

ABSTRACT

Due to their high aspect ratio, strength, and modulus, multiwall carbon nanotubes (MWCNT) have attracted interest as a reinforcing filler in the automotive tire industry. In part 1 of this study, we demonstrated that styrene–butadiene rubber (SBR) composites containing up to 15 wt. % of well-dispersed, discrete MWCNTs can be prepared using MWCNTs with a specific surface modification and controlled aspect ratios. The melt rheology of the composites with discrete MWCNT was best described in terms of an effective aspect ratio and by considering the discrete MWCNT to be flexible rather than rigid rods. In this work, the effect of tensile strains, up to values of 6, for cured SBR composites containing discrete MWCNT concentrations up to 12% by weight were investigated. The deformation behavior indicates good adhesion between these MWCNT and the SBR. Mooney–Rivlin plots derived from the composite tensile stress–strain data displayed a dramatic change in mechanical behavior as the MWCNT loading exceeded about 5 wt. % attributed to a combined reinforcing effect of tubes on SBR plus overlap of curved or coiled MWCNT. Beyond tensile strains of about 1.7, strain hardening increases dramatically at MWCNT loading greater than 5 wt. % that is attributed to straightening of the initially curved nanotubes such that they behave as rigid rods or fibers. Mechanical hysteresis and swelling in toluene on cured composites samples revealed that MWCNTs are in fact well bonded to the SBR. Studies with SBR and a combination of carbon black and discrete MWCNT demonstrate dramatically improved resistance to fracture by tearing.

© 2014 Elsevier Ltd. All rights reserved.

1. Introduction

Styrene–butadiene rubber, SBR, is widely used as one of the components of the elastomeric matrix for automotive tires [1,2], as well as for wire and cable applications, and sporting goods. For enhanced performance of tires, SBR composites should possess good mechanical properties including improved wear and tear resistance. SBR is most often blended with other rubbers such as natural rubber and poly(cis-butadiene) for specific applications. Various combinations of conventional fillers with low aspect ratios such as carbon black, silica, and clays, etc., have been employed to enhance mechanical [1,3–8], barrier [9–13] and tear properties. Typically, such composites contain high loadings of these conventional fillers up to 60 parts per hundred of rubber, phr [14]. It is also well recognized that polymer–filler composites with such loadings

invariably involve some agglomeration of particles due to poor interaction between the polymer and the particle surface plus strong interparticle interactions [15]. These agglomerates can cause deterioration of properties such as wear resistance.

When a tire tread undergoes cyclic loading and strains in actual use, nano-sized voids form at stress concentration locations at and between filler–elastomer interfaces. Under repetitive loading, these voids can coalesce and grow in size to form micron-sized cracks; this eventually leads to failure of the tire. A number of crack propagation mechanisms have been proposed in the literature for elastomers [16–20] demonstrating how cracks form in elastomer composites loaded with conventional fillers such as carbon black (CB) and/or silica. Multiple efforts have been made to prevent the propagation of nano-sized voids into micron-sized cracks and to further enhance the mechanical properties of the composite by adding a small amount of multiwall carbon nanotubes (MWCNT) [21–23]. The MWCNTs are anticipated to act as crack bridging elements due to their high aspect ratios and their inherent high tensile modulus (1 TPa) and strength (50–500 GPa)

* Corresponding author.

E-mail address: ellison@che.utexas.edu (C.J. Ellison).

[24–27]. The basic requirements for the MWCNT to act as crack initiation and growth inhibitors include being well-dispersed and having good adhesion or being bonded to the matrix. However, since rubbers such as SBR may be deformed to high strains, the fillers have to accommodate these high strains without causing premature failure within the rubber phase.

In previous studies, even though MWCNT-filled elastomers exhibit some improvement in tensile properties, they generally do not reach their expected performance based on the properties of the tubes themselves. This may be attributed primarily to lack of discrete MWCNT, poor MWCNT dispersion and weak tube-to-matrix surface adhesion [28].

Part 1 of this series reported a process for making masterbatches containing up to 15 wt. % of discreet, well-dispersed MWCNTs in a SBR matrix using an emulsion coagulation technique [29]. The concentrated masterbatches could be diluted with SBR to give lower MWCNT loadings while preserving excellent tube dispersion. A key to this technology is proper surface functionality and controlling tube aspect ratio at an optimum level to achieve rheological properties that permit processing while preserving good mechanical properties. In particular, the carbon nanotubes were observed to be highly curved or coiled and as such, an effective aspect ratio determined from the overall tube contour length to end–end distance was found to be a more relevant parameter to relate to the composite rheology under various strain rates. The changes in effective aspect ratio with dilution indicates that the tubes are best considered as being flexible rather than rigid rods.

In this study, composites made by curing nanocomposites formed by dilution of such a masterbatch will be used to investigate the tensile and tear properties. Mechanical hysteresis experiments on these cured composites are performed to understand the interactions between MWCNT and SBR. These results are further supported by swelling studies in toluene. These studies form a basis for future work on MWCNT composites based on blends of rubber of the type used in commercial tires; further papers will discuss the mixing rules of various masterbatches, rheology, and various mechanical properties.

2. Experimental

2.1. Materials

The multiwall carbon nanotube/SBR composites studied here were prepared from a MWCNT/SBR masterbatch prepared by a coagulation process followed by melt mixing in a high shear twin-

screw extruder. The masterbatch was then diluted to various carbon nanotube concentrations with additional SBR plus curing additives by melt compounding in a Haake batch mixer. These mixed masterbatches were pressed into sheets and cured as described previously [29]. The pure MWCNTs and CB had specific surface areas of 200 and 110 m²/g, respectively.

2.2. Mechanical measurements

Tensile measurements on composite samples were made at room temperature according to ASTM D 412-06 using an Instron™ 3360 Series Dual Column testing system equipped with an extensometer. The gage length was 33 mm. These measurements were performed on samples cut as shown schematically in Fig. 1a. Crosshead stretch rate for the stress vs. strain measurements was 500 mm/min; whereas for hysteresis measurements, the rate was 50 mm/min. Hysteresis at variable strain rate measurements on a single specimen of a composite sample were started at 50 mm/min and, then increased incrementally to 200 mm/min in 50 mm/min increments. The stress vs. strain data were processed with Bluehill™ software.

Constrained tear testing was carried out on specimens cut into rectangular strips of 50.8 × 25.4 × 2 mm³ with a notch cut to a depth of 12.7 mm as shown in Fig. 1b. The specimen was held between the grips with a constrained sample area measuring 25.4 × 25.4 mm² with the notch at equal distances from the grips. A stretch rate of 25.4 mm/min was used for these tests.

2.3. Swelling studies

Equilibrium swelling measurements of composite specimens were performed on rectangular samples with dimensions 20 × 10 × 2 mm³ soaked in toluene for 72 h. Sample dimensions (length, width, and thickness) were measured with calipers accurate to 0.01 mm, as well as sample mass, before and after swelling and then after drying. The equilibrium swelling ratios (Q_v) were determined from the sample specimen volumes and by calculations from sample mass using appropriate densities.

$$Q_v = \left(\frac{\text{volume of swollen specimen}}{\text{volume of original unswollen specimen}} \right) \quad (1)$$

3. Results and discussion

Tensile stress–strain curves for cured SBR composites containing from 1 to 12.3 wt. % MWCNT are shown in Fig. 2a and compared with cured SBR. As expected, the stress levels of the composites increase with MWCNT loading at all strains. From a loading of 4–5 wt. % MWCNT and above, the stress vs. strain curves become more linear compared with those at lower MWCNT concentrations. To further understand these tensile results, the data are recast in the form of a reduced stress, σ_r , versus reciprocal extension ratio, $1/\lambda$, or a Mooney–Rivlin plot, as shown in Fig. 2b. The rationale for such plots is the following equation from the phenomenological theory of rubber elasticity [18,30–37] in the absence of any filler.

$$\sigma_r = \frac{\sigma}{\left(\lambda - \frac{1}{\lambda^2}\right)} = 2C_1 + \frac{2C_2}{\lambda} \quad (2)$$

The reduced stress is defined as the engineering stress, σ , divided by the strain function, $\lambda - 1/\lambda^2$, suggested by the molecular theory of rubber elasticity [30,32,38,39], where $\lambda = (L/L_0) = 1 + \epsilon$, and L and L_0 are the final and initial lengths, and ϵ is the tensile strain. The terms C_1 and C_2 are expected to be constants with C_1

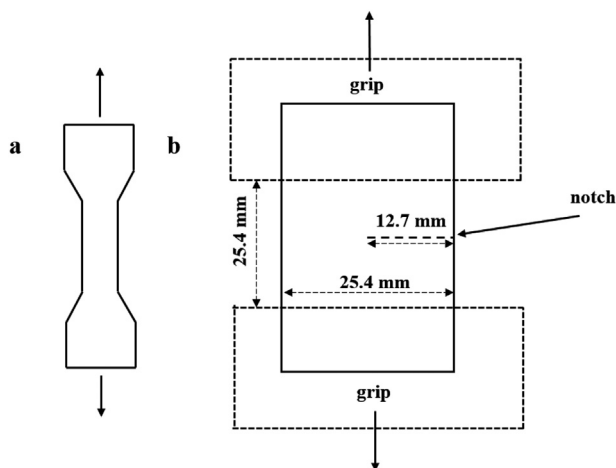


Fig. 1. Schematic representations of a) tensile, and b) constrained tear test specimens.

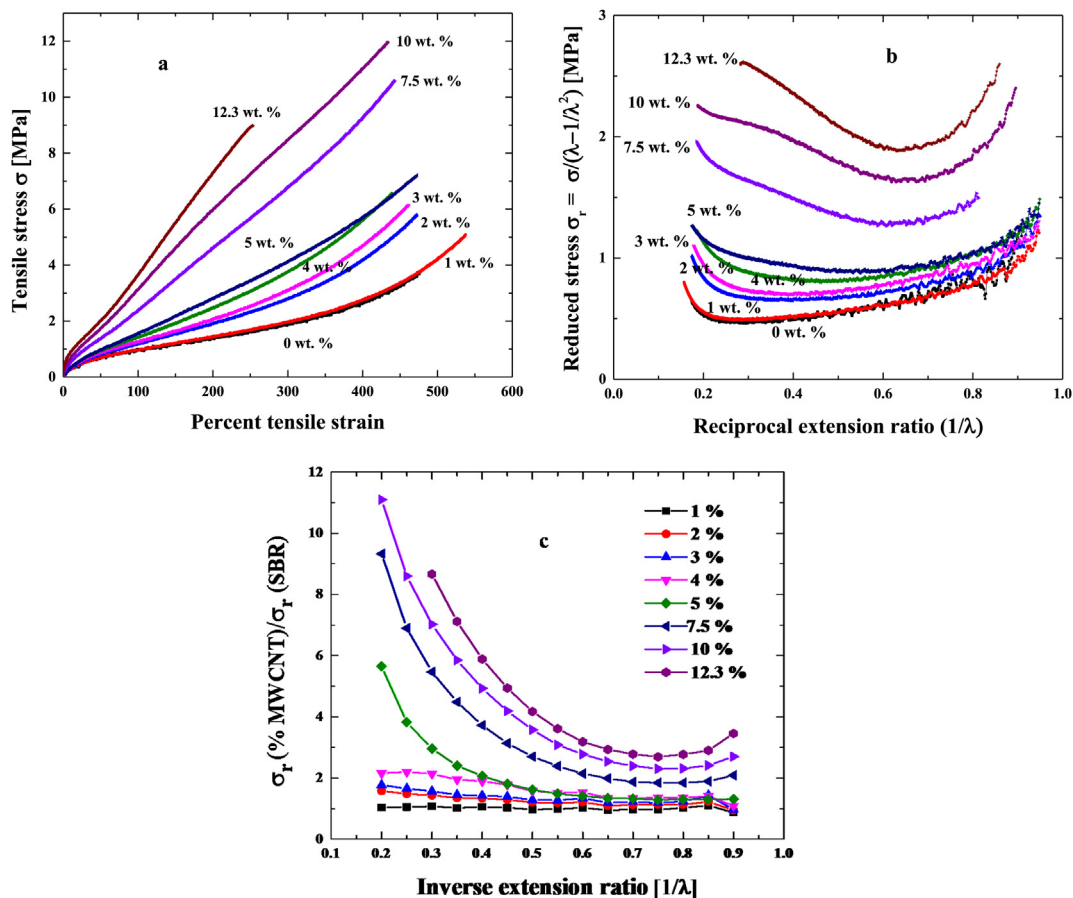


Fig. 2. a) Tensile stress–strain responses of SBR composites containing different loadings of MWCNT, b) Mooney–Rivlin curves from the tensile stress–strain data, c) Mooney–Rivlin plot of the data where the reduced stress of the composites has been divided by that of the cured SBR without MWCNT.

related to the crosslink density for elastomers without filler. In Fig. 2c, the reduced stress values for the nanocomposites have been normalized with the reduced stress observed for SBR at the same strain. This helps separate contributions from the MWCNT and from the SBR network.

The Mooney–Rivlin plots can be divided into the following three regions of strain: low strain ($1/\lambda > 0.8$), intermediate strain and high strain where the boundary between the latter two shifts with MWCNT loading. Before interpreting these plots it is important to remember that the stress–strain behavior recorded was taken at finite extension rates (500 mm/min) and are, thus, not equilibrium curves but rather reflect some level of viscoelastic response. The Mooney–Rivlin response for the unfilled SBR sample (black) as shown in Fig. 2b has a linear region from $1/\lambda = -0.25$ to 0.8. All of the samples show some non-linearity on these coordinates in the lower strain region, $1/\lambda > 0.8$ including SBR without MWCNT. The curvature in this region for the composites containing up to 4 wt. % MWCNT is due entirely to the response of the SBR matrix as made clear in Fig. 2c. For large strains $1/\lambda < 0.25$, the SBR sample shows upward curvature as strain is increased; and this can be attributed to the non-Gaussian nature of the molecular network [38,40,41]. This, in turn, is also seen in the curves for the composites with 4 wt. % MWCNT or less. The stress values at all strains increase as the content of MWCNT increases owing to reinforcement or a “strain amplification” effect, as expected for any rigid filler. What is most remarkable about the trends seen most clearly in Fig. 2c is the dramatic rate of increase in stress with added MWCNT that occurs around 5 wt. %. Interestingly, this is near the same MWCNT content

where an increase in slope of a plot of viscosity vs MWCNT loading was observed earlier [29]. This threshold composition between 4 and 5 wt. % MWCNT (or about 2.6 vol. %) was previously interpreted in the context of the viscosity as delineating two regimes of nanotube dispersion where at lower concentrations the tubes exist more or less individually while at higher contents the coils of the tubes overlap. The transition may be thought of as analogous to the onset of entanglements of polymer chains or the coil–coil overlap in polymer solutions represented in the schematic shown in Fig. 3 [42]. It appears that a similar effect may be at play in the mechanical deformation of these cured composites.

The upturn of the reduced stress at high strains (see Fig. 2b) begins at lower strains as the loading of MWCNT increases beyond 4–5 wt. %. The upturn at low strains also extends to higher extension ratios. These two effects combined lead to a severe departure from the linear response expected in the classical Mooney–Rivlin plot and observed at low MWCNT loadings. The shifting of the high strain upturn to lower extension ratios may reflect the presence of shorter network chains (formed during the vulcanization process particularly those involving SBR bound to the MWCNT) with increasing MWCNT loading. Of course, the upturn also has to reflect the uncoiling of the curved or coiled MWCNT that apparently occurs at lower strains with higher MWCNT loading, resulting from more extensive tube–tube overlap.

Values of tensile stress at break and elongation at break for these composites were averaged for at least 5 samples and are shown in Fig. 4a and b. The initial modulus plus tensile stress at 100% strain are also shown in Table 1. As seen in Fig. 4a, the tensile stress at

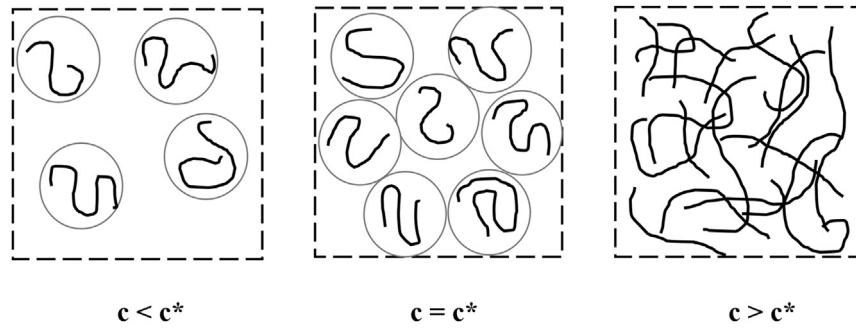


Fig. 3. Schematic representing overlapping of coils of tubes with increasing MWCNT loading [42].

break increases with increasing MWCNT loading up to 10 wt. % and then appears to decrease after that. This increase reflects the reinforcing effect of a filler with high modulus and strength and good SBR-MWCNT surface bonding between the MWCNT and SBR. There is also very definite evidence of a change in response of the elongation at break around 6–8 wt. %, see Fig. 4b.

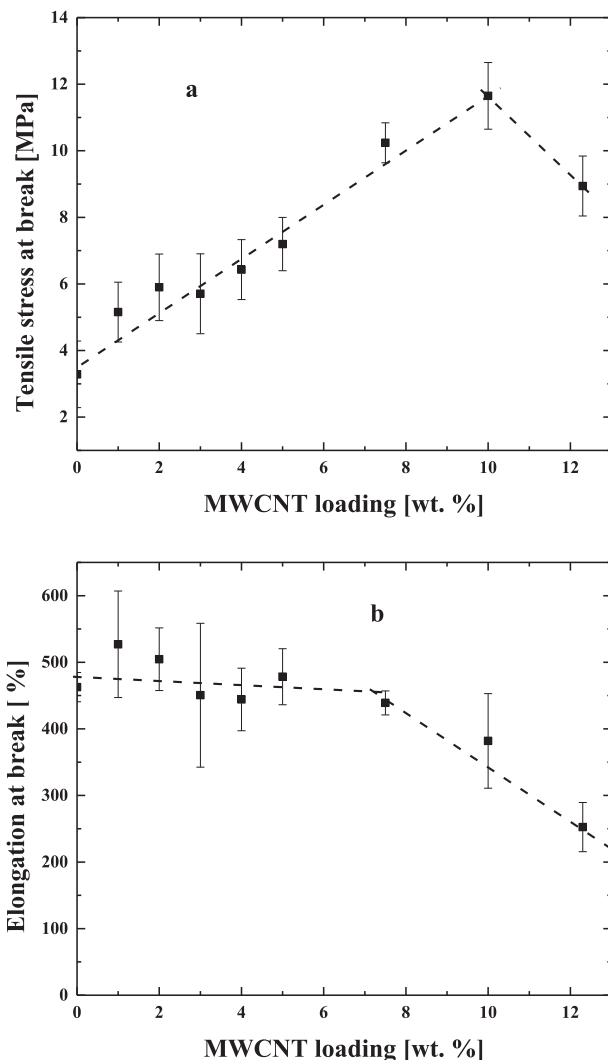


Fig. 4. a) Tensile stress at break, b) elongation at break as a function of MWCNT loading (dashed lines drawn to guide the eye).

The average elongation at break values for the composites are very close to that of SBR (~450%) up to the loading level of the proposed threshold. It is remarkable to see essentially no decrease in elongation at break with addition of MWCNT below this threshold; this is even more remarkable given the significant improvements in the tensile stress at break observed. The reason behind the high elongation at break reflects two inter-related factors; one is a strong interfacial bonding between SBR and tube surface and the other is straightening of the curved or coiled tubes in the stretch direction along with the matrix as schematically shown in Fig. 5a and b. At higher MWCNT loadings, the elongation at break shows a modest decrease. The high aspect ratio of the MWCNT permits a high degree of load sharing with the rubber matrix and as crack bridging elements that prevent failure at low stresses. The high elongation at break for these composites is, in part, the result of uncoiling of MWCNTs in the SBR matrix. Of course, such responses are only possible if there is excellent physical and/or chemical interactions between tube surface and rubber. These interactions between the filler and rubber act, in part, as physical crosslink points. At high enough loadings of MWCNT, these “effective” physical crosslinks would act as barriers to the deformation of SBR, leading to the reduced elongation at break [43] and tensile stress values after 10 wt. % observed in Fig. 4a.

Insights about irreversible changes in the structure of rubber composites can be gained by performing multiple load cycles (or hysteresis). Grosch et al. [44] and Harwood and Payne [45,46], for example, have studied the hysteresis properties of rubbers filled with carbon black at high strains. Their findings suggest that the greater the area under the stress–strain curve, i.e., the energy that a rubber dissipates while stretching, the more energy the rubber can withstand before breaking. The Mullins hysteresis [39,47–51] or the strain-softening effect is quite commonly observed in elastomers filled with carbon black or MWCNTs. When these elastomer-filler composites are exposed to multiple cycles of loading, the area under the first stretch stress–strain curve is different from the retraction curve, and this difference has been attributed to several

Table 1
Tensile properties of SBR-MWCNT composites.

Sample name	Tensile stress at break [MPa]	Elongation at break (%)	Tensile stress at 100% [MPa]	Initial modulus [MPa]
SBR	3.3 ± 1.0	463 ± 22	1.0 ± 0.03	1.9 ± 0.5
1%	5.2 ± 0.9	527 ± 80	0.9 ± 0.04	1.9 ± 0.5
2%	5.9 ± 1.0	505 ± 47	1.0 ± 0.11	2.1 ± 0.4
3%	5.7 ± 1.2	451 ± 108	1.2 ± 0.11	2.3 ± 0.3
4%	6.4 ± 0.9	444 ± 47	1.4 ± 0.06	2.6 ± 0.3
5%	7.2 ± 0.8	478 ± 42	1.5 ± 0.18	2.5 ± 0.3
7.5%	10.2 ± 0.6	439 ± 18	2.3 ± 0.10	3.6 ± 0.2
10%	11.7 ± 1.0	382 ± 71	3.4 ± 0.55	4.5 ± 0.5
12.3%	8.9 ± 0.9	252 ± 37	3.7 ± 0.21	5.4 ± 0.2

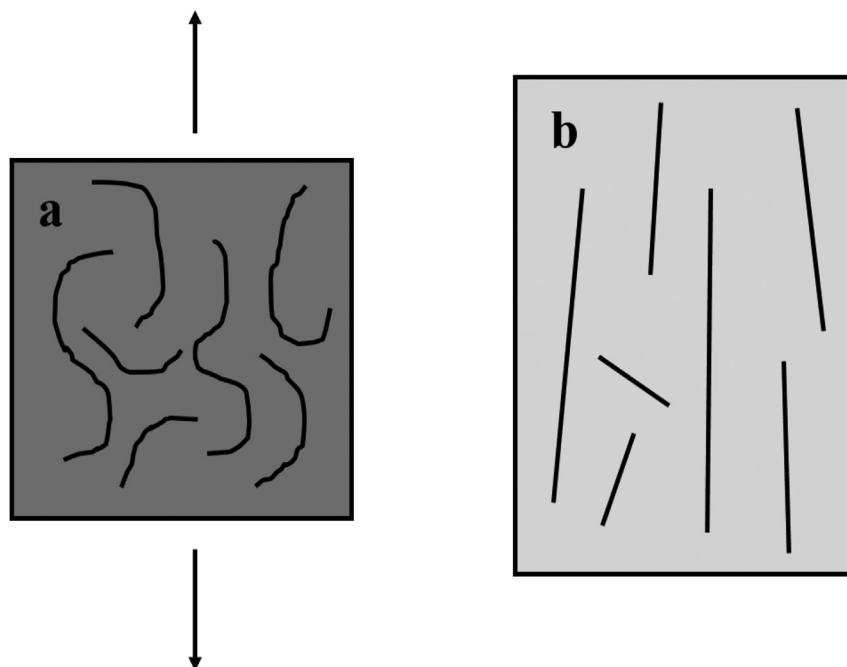


Fig. 5. a) Composite sample with coiled MWCNTs before stretching, and b) stretched sample with straight MWCNTs.

possible causes including the breakage or the slippage of chains from the particle surface which has reached the limit of extensibility [50–52]. Specimens of SBR and its composites were stretched in this study four times in a tensile mode to a specific strain prior to the breaking strain of the sample. A 200% strain was chosen for an

SBR sample while for SBR-MWCNT composites it was chosen as 150% to avoid breaking during multiple stretches. Some composites containing MWCNT failed prematurely when stretched multiple times to 200%, hence 150% was chosen as a safety limit for composites containing MWCNT in these hysteresis experiments. At the

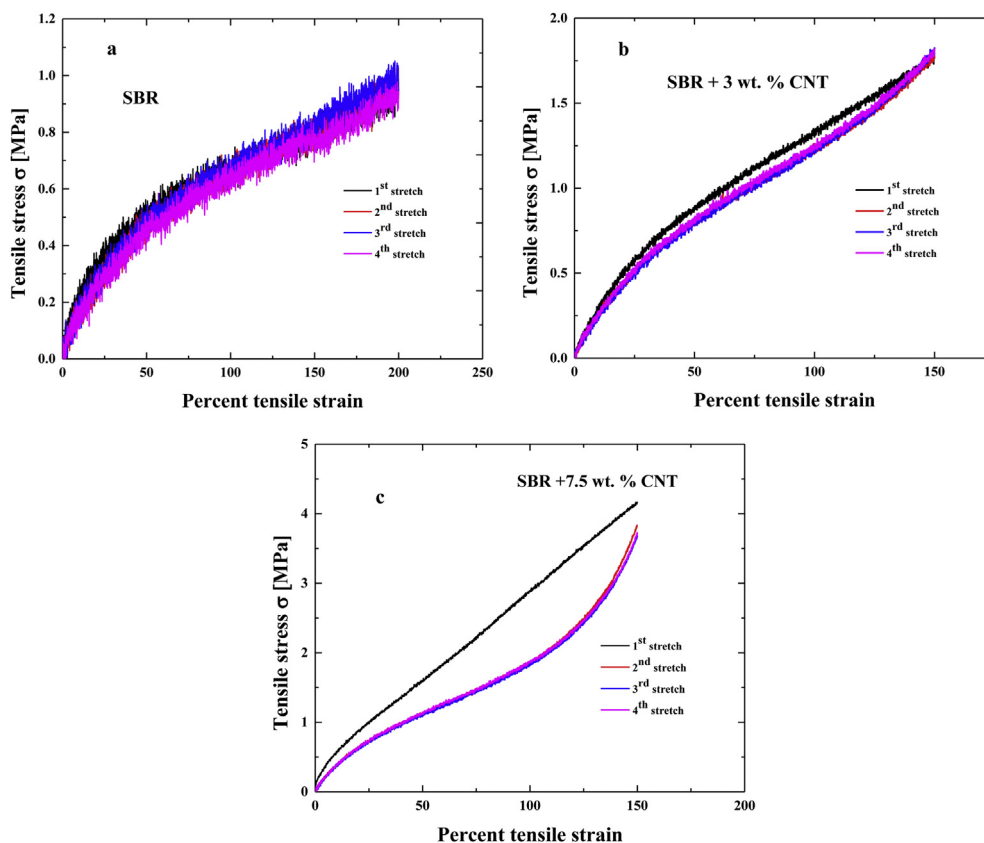


Fig. 6. Tensile stress–strain loading responses for a) SBR, b) 3 wt. % CNT-SBR, and c) 7.5 wt. % CNT-SBR composite samples, respectively.

end of each final stretch, samples were equilibrated at that stretch for 15 min before re-stretching. Fig. 6a shows stress–strain curves obtained by multiple stretches for a cured SBR sample without any MWCNT. From this, it is clearly evident that there is no substantial difference observed in the successive stress–strain curves for the SBR sample; this suggests there is no significant chain breakage.

The stress–strain data from the first and second stretches for 3 and 7.5 wt. % MWCNT loaded SBR composites are shown in Fig. 6b and c, respectively. For the composite containing 3 wt. % MWCNT, the second stress–strain response differs slightly from the first stretch whereas for the composite containing 7.5 wt. % MWCNT, there is a significant difference between the first and second stress–strain responses. This is similar to the well-known Mullin's hysteresis or strain-softening effect commonly observed for rubber composites [47].

Some part of the hysteresis observed in the present composites may be the result of irreversible re-arrangement or straightening of

the MWCNTs. At loadings higher than the threshold concentration for overlapping of tubes, akin to coil–coil overlapping as observed in polymer chains in solution [42], such effects are apparently more exaggerated. Note that the third and fourth stretches are quite similar to the second stretch. This indicates that the initial re-arrangements of the composites only happen during the first stretch and from the second stretch onwards no further changes are significant provided the composite is not stretched to a higher strain level. Similar, but more exaggerated, responses were also observed for 10 and 12.3 wt. % MWCNT filled SBR composites (see the Supporting Information).

The first and second stretch stress–strain curves for SBR, and composites containing various amounts of MWCNT represented as Mooney–Rivlin plots are shown in Fig. 7a–e. At lower levels of strains, the reduced stress levels in the second stretch are lower than that of the first stretch at low extensions. This is true for SBR without any nanotubes; this effect is not so apparent at low

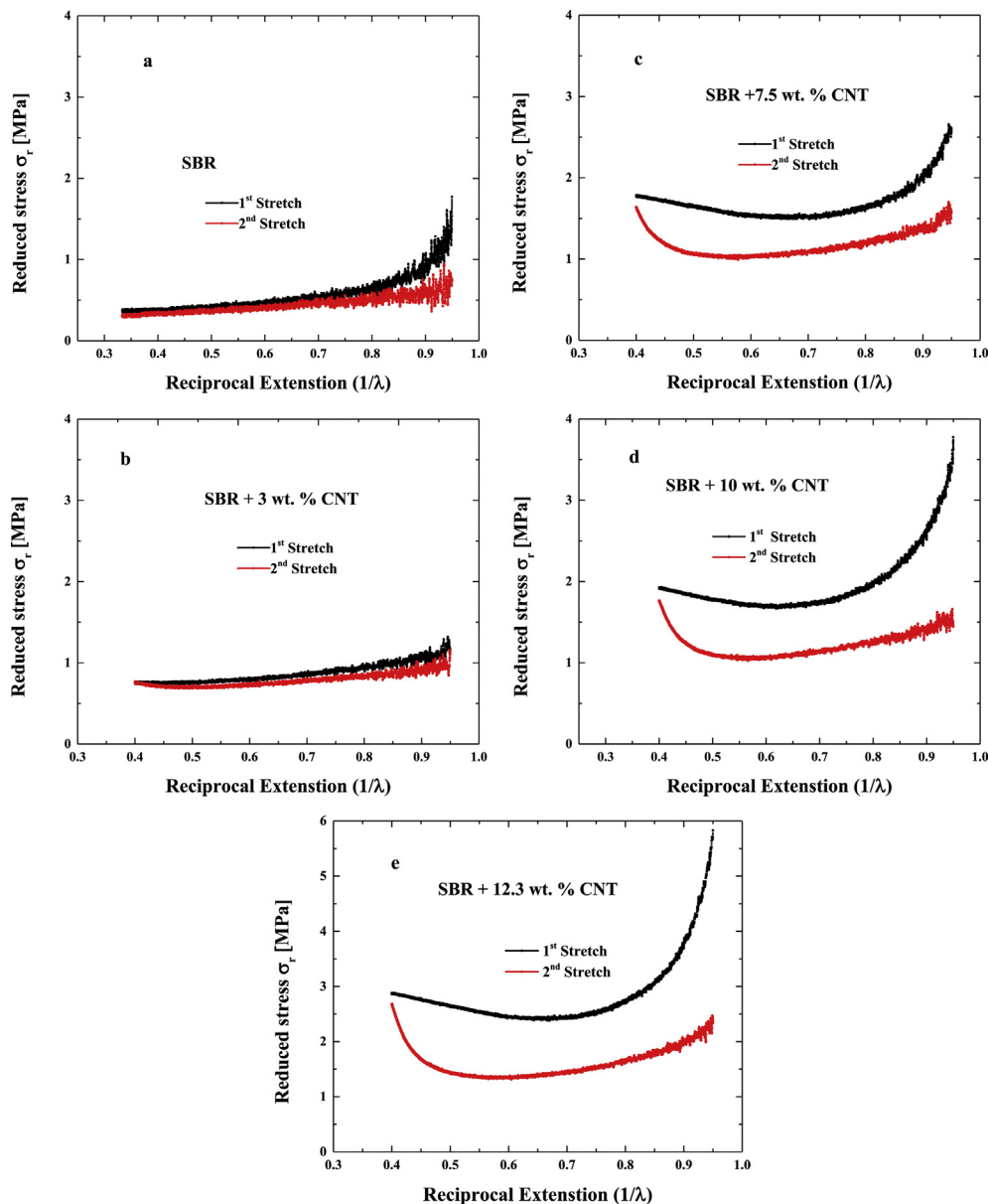


Fig. 7. Mooney–Rivlin curves derived from first and second stress–strain loading responses for a) SBR, b) 3 wt. % CNT-SBR, c) 7.5 wt. % CNT-SBR, d) 10 wt. % CNT-SBR, and e) 12.3 wt. % CNT-SBR composites, respectively.

loadings of MWCNT but became much more significant with MWCNT loadings >5 wt. %. As the strain levels approach 150% or $1/\lambda = 0.4$, the reduced stress in the second stretch approaches the value of the first stretch. At this strain, the sample in the second stretch has the same load bearing structure achieved when it was first stretched to this strain; similar behavior is observed in other rubber-filler composites [52–54].

Further understanding of hysteresis of MWCNT-filled SBR was carried out by stretching samples multiple times to different strains and with subsequent comparison of stress–strain curves for a sample that was stretched continuously to the highest strain. Fig. 8a and b represent the hysteresis behavior of SBR and SBR filled with 7.5 wt. % MWCNT composites, respectively. Similar responses were observed for 3 and 12.3 wt. % MWCNT composites (Shown in Supporting Information). In Fig. 8a, the data for all stretches (first, second and third) of SBR that were stretched to 100, 150, and 200% essentially fall on top of each other. Furthermore, data from the continuous stretch to 200% of a fresh SBR specimen matches with that of the above mentioned sequence. This indicates that there is essentially no significant hysteresis for the SBR sample even when stretched multiple times to different strains. However, a sample containing 7.5 wt. % MWCNT displays significant strain-softening

when it was stretched multiple times as shown in Fig. 8b. This reflects continuous structural rearrangements that occur on stretching, and when subsequently re-stretched the arrangement process continues when the strains exceed those of previous stretches. This illustrates that these MWCNT composites behave very similar in this regard as other rubber composite.

Constrained tear measurements were performed in a tensile mode on SBR as well as composites filled with CB and with CB plus MWCNT. Fig. 9a shows the apparent stress vs strain relation for each of the materials mentioned as the samples were loaded to failure. The area under the tear stress–strain curve represents the amount of work (or energy) required to tear the respective sample to complete failure. SBR filled with 40 phr CB fails at 100% strain with a classical breakdown of CB–CB particle structure associations in a step-wise pattern before complete failure of the specimen [18,55–57]. Addition of 3 phr MWCNT to a sample containing 40 phr CB in SBR caused a further increase in tear properties compared with CB filled SBR composite; this material extends to over 150% strain, much like the unfilled SBR, before complete failure. The lack of a step-wise breakdown of structures in the tear initiation curve and the higher area under the curve (i.e., more energy required to break the sample) indicates the MWCNTs are

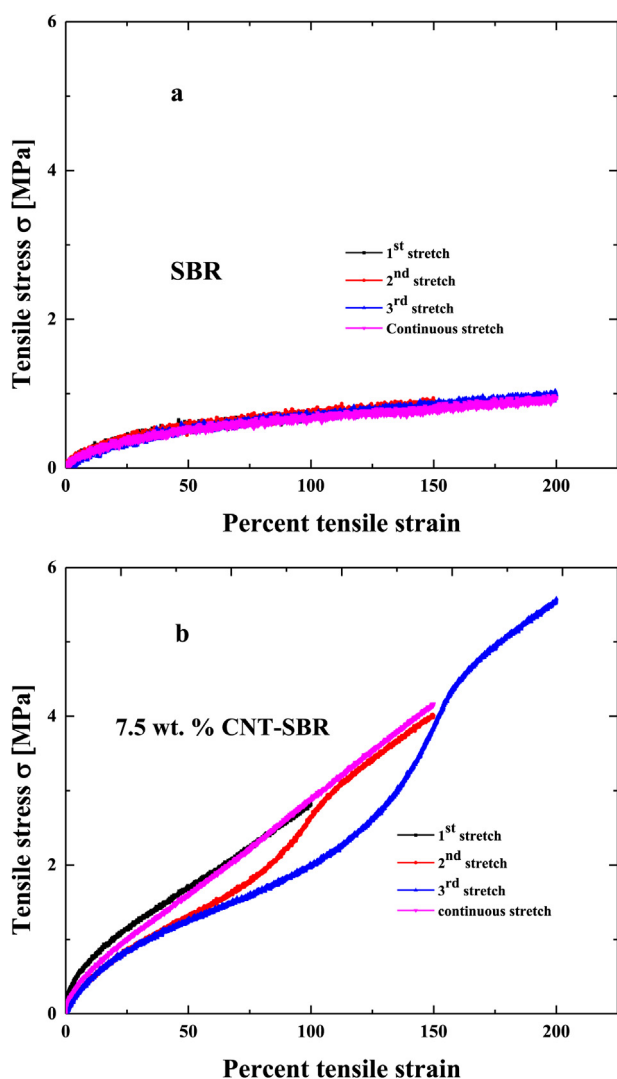


Fig. 8. Hysteresis (tensile stress–strain response) curves for a) SBR composite, b) SBR filled with 7.5 wt. % MWCNT composite.

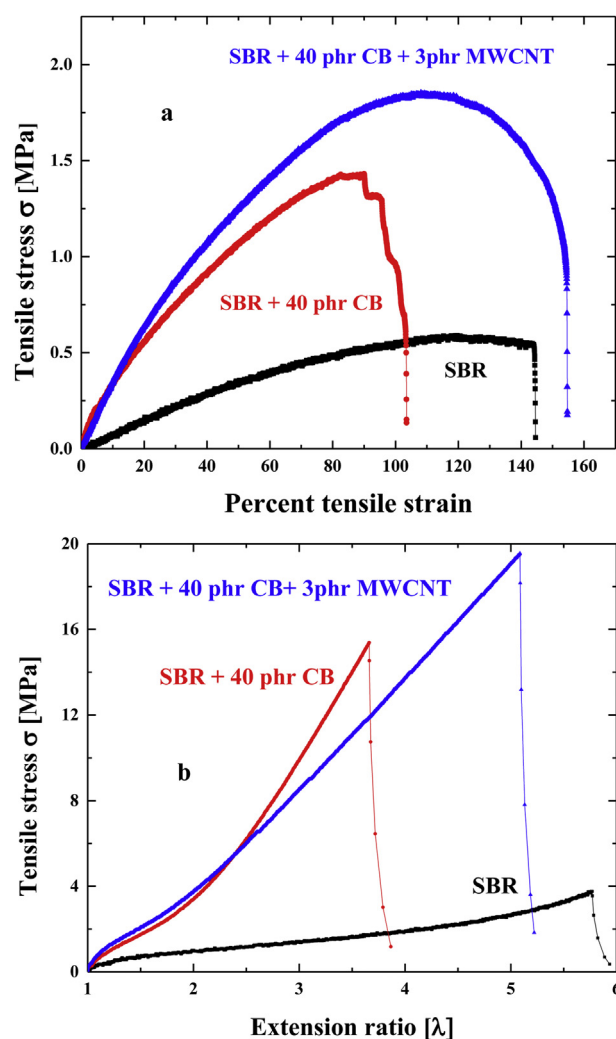


Fig. 9. Plots of a) Tensile stress vs. strain in constrained tear mode (with notch), b) tensile stress vs. extension ratio in tensile mode responses (without notch) for SBR, SBR filled with CB and, CB and MWCNT, respectively.

Table 2
Constrained tear testing (with notch) results for composites of SBR filled with CB and CB + MWCNT.

Sample	Stress at break [MPa]	Elongation at break [%]	Area under the curve [MPa]
SBR	0.3 ± 0.06	184 ± 12	0.7 ± 0.04
SBR + 40 phr CB	0.6 ± 0.06	109 ± 5	1.1 ± 0.1
SBR + 40 phr CB + 3 phr MWCNT	0.8 ± 0.06	144 ± 7	2.0 ± 0.1

Table 3
Tensile testing (without notch) results for composites of SBR filled with CB and CB + MWCNT.

Sample	Tensile stress at break [MPa]	Elongation at break [%]	Modulus [MPa]
SBR	3.3 ± 1.0	463 ± 22	1.9 ± 0.5
SBR + 40 phr CB	15.5 ± 1.2	273 ± 0.2	8.3 ± 0.2
SBR + 40 phr CB + 3 phr MWCNT	19.5 ± 1.2	407 ± 0.2	5.4 ± 0.1

indeed acting as crack bridging elements for inhibiting tear propagation. Table 2 shows stress and strain at break for these samples plus the energy to break. Relative to unfilled SBR, the addition of CB causes ~60% increase in tear energy while adding both CB and MWCNT causes a 2.8-fold increase. Tensile stress vs. strain measurements were also performed on the samples of the same compositions as for constrained tear tests, but without the notch. The stress–strain curves for the three samples are shown in Fig. 9b with results summarized in Table 3.

An important message from these tensile measurements is that addition of MWCNT to SBR/CB composites causes failure to occur at higher stresses and higher elongations; this may be attributed to the unique reinforcing characteristics of MWCNT combined with strong surface interactions between the MWCNT and SBR. Higher elongations at break are attributed to the uncoiling of curved MWCNTs during the stretching process as shown schematically in Fig. 5a and b.

An indirect correlation of SBR and MWCNT surface interactions was explored using swelling of the composite specimens in toluene. Fig. 10 shows the swelling ratio (Q_v) curves for the

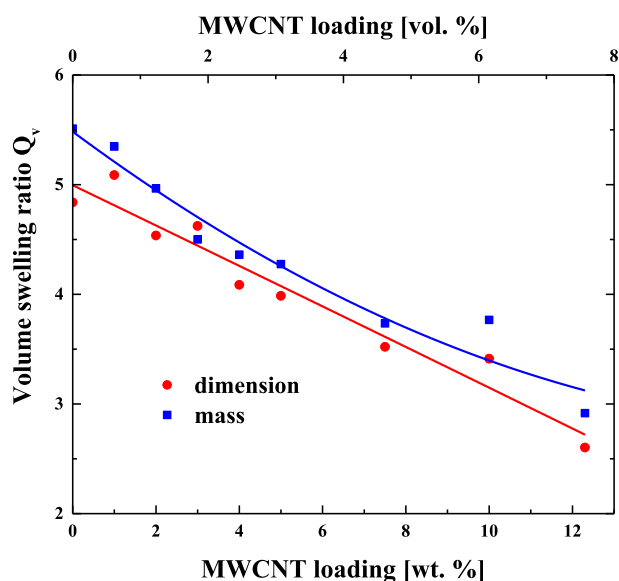


Fig. 10. Swelling ratio for composites in toluene calculated from volumes and masses as a function of MWCNT loading.

composite samples calculated from the volumes and masses as a function of MWCNT loading. It can be seen that Q_v in both curves (calculated from the masses and volumes of samples) strongly decreases with increasing MWCNT loading. The swelling ratios calculated using mass and volume determinations differ slightly perhaps owing to differences in techniques and accuracy; however, the trends are clear. This decrease in swelling with increasing MWCNT loading is due to strong bonding between the SBR and MWCNT surfaces such that the MWCNT are able to constrain the extent to which the SBR network can swell.

4. Conclusions

Tensile stress–strain measurements were performed on cured SBR samples containing various loadings of MWCNT. The elongation at break remained at the level of SBR (~460%) until about 7.5 wt. % MWCNT and then decreased slightly while the stress at break increased by 210% up to 7.5 wt. % MWCNT reflecting the reinforcing effect of MWCNT and its interactions with SBR. Mooney–Rivlin plots derived from the tensile stress–strain curves show that the curves shift towards higher reduced stress values with increasing MWCNT loading due to reinforcement of SBR. Multiple stress–strain measurements on the same composite sample showed significant hysteresis, e.g., Mullin's strain-softening behavior, for samples containing MWCNT. The stress–stress responses from the second stretch onwards (third and fourth stretches) rejoin the stress–strain curve of a first stretch at higher strain levels. This reflects continuous irreversible structural rearrangements of the composite that continue when subsequent strains exceed the strain applied in the previous stretch. When the specimen is stretched to higher strains, it responds like a fresh specimen from that point. Reduction in swelling ratios of rubber in toluene, determined from both volume and mass measurement, with increasing MWCNT loading demonstrates a significant constraint by the MWCNT that can be attributed to a good interfacial interaction between MWCNT surface and the SBR matrix. In many ways, the MWCNT composites show similar mechanical behavior to CB composites, but at significantly lower loadings of MWCNT.

Constrained tear testing on sample filled with CB and with both CB and MWCNT were performed. Compared with unfilled SBR, the addition of CB causes ~60% increase in tear energy while adding both CB and MWCNT causes a 2.8-fold increase indicating that the MWCNTs act as effective crack bridging elements.

Acknowledgments

The authors would like to thank Dr. M.F. Finlayson for preparing the initial masterbatch and Macon Leighton for helping with the tear testing. The authors also like to thank Molecular Rebar Design, LLC for funding this project and instrumentation support.

Appendix A. Supplementary data

Supplementary data related to this article can be found online at <http://dx.doi.org/10.1016/j.polymer.2014.11.006>.

References

- [1] Boonstra BB. *Polymer* 1979;20(6):691–704.
- [2] Heinrich G, Kluppel M, Vilgis TA. *Curr Opin Solid State Mater Sci* 2002;6(3):195–203.
- [3] Alexandre M, Dubois P. *Mater Sci Eng R-Rep* 2000;28(1–2):1–63.
- [4] Allaoui A, Bai S, Cheng HM, Bai JB. *Compos Sci Technol* 2002;62(15):1993–8.
- [5] Ambacher H, Strauss M, Kilian HG, Wolff S. *Kautsch Gummi Kunstst* 1991;44(12):1111–8.

- [6] Bergstrom JS, Boyce MC. Rubber Chem Technol 1999;72(4):633–56.
- [7] Biswas M, Ray SS. Recent progress in synthesis and evaluation of polymer-montmorillonite nanocomposites. In: Abe A, Albertsson AC, Cantow HJ, Dusek K, Edwards S, Hocker H, et al., editors. New polymerization techniques and synthetic methodologies, vol. 155. Berlin: Springer-Verlag; 2001. p. 167–221.
- [8] Ramanathan T, Liu H, Brinson LC. J Polym Sci Part B-Polym Phys 2005;43(17):2269–79.
- [9] Perez LD, Zuluaga MA, Kyu T, Mark JE, Lopez BL. Polym Eng Sci 2009;49(5):866–74.
- [10] Lu Y-L, Li Z, Yu Z-Z, Tian M, Zhang L-Q, Mai Y-W. Compos Sci Technol 2007;67(14):2903–13.
- [11] Stephen R, Ranganathaiah C, Varghese S, Joseph K, Thomas S. Polymer 2006;47(3):858–70.
- [12] Wang ZF, Wang B, Qi N, Zhang HF, Zhang LQ. Polymer 2005;46(3):719–24.
- [13] Bhattacharya M, Biswas S, Bhowmick AK. Polymer 2011;52(7):1562–76.
- [14] Bokobza L, Rapoport O. J Appl Polym Sci 2002;85(11):2301–16.
- [15] Herd CR, McDonald GC, Hess WM. Rubber Chem Technol 1991;65(1).
- [16] Previati G, Kaliske M. Int J Fatigue 2012;37(0):69–78.
- [17] Aglan H, Chudnovsky A, Moet A, Fleischman T, Stalnaker D. Int J Fract 1990;44(3):167–78.
- [18] Rivlin RS, Thomas AG. J Polym Sci 1953;10(3):291–318.
- [19] Thomas AG. J Polym Sci 1955;18(88):177–88.
- [20] Thomas AG. Rubber Chem Technol 1994;67(3):G50–60.
- [21] Das A, Stockelhuber KW, Jurk R, Saphiannikova M, Fritzsche J, Lorenz H, et al. Polymer 2008;49(24):5276–83.
- [22] Bhattacharyya S, Sinturel C, Bahloul O, Saboungi M-L, Thomas S, Salvétat J-P. Carbon 2008;46(7):1037–45.
- [23] Sohi NJS, Bhadra S, Khastgir D. Carbon 2011;49(4):1349–61.
- [24] Xie X-L, Mai Y-W, Zhou X-P. Mater Sci Eng R Rep 2005;49(4):89–112.
- [25] Salvétat J, Bhattacharyya S, Pipes RB. J Nanosci Nanotechnol 2006;6(7):1857–82.
- [26] Byron Pipes R, Frankland SJV, Hubert P, Saether E. Compos Sci Technol 2003;63(10):1349–58.
- [27] Tu Z, O-Y Z. Phys Rev B Condens Matter 2002;65(23).
- [28] Thess A, Lee R, Nikolaev P, Dai HJ, Petit P, Robert J, et al. Science 1996;273(5274):483–7.
- [29] Peddini SK, Bosnyak CP, Henderson NM, Ellison CJ, Paul DR. Polymer 2014;55(1):258–70.
- [30] Mooney M. J Appl Phys 1940;11(9):582–92.
- [31] Rivlin RS. Nature 1948;161(4093):567–8.
- [32] Rivlin RS. Proc Roy Soc Lond Math Phys Sci 1948;193(1033):261–81.
- [33] Rivlin RS. Phil Trans Roy Soc Lond Math Phys Sci 1948;240(822):459–508.
- [34] Rivlin RS. Phil Trans Roy Soc Lond Math Phys Sci 1948;241(835):379–97.
- [35] Rivlin RS. Phil Trans Roy Soc Lond Math Phys Sci 1948;240(823):509–25.
- [36] Rivlin RS. Proc Camb Phil Soc 1948;44(4):595–7.
- [37] Treloar LRG, Hopkins HG, Rivlin RS, Ball JM. Proc Roy Soc Lond Math Phys Sci 1976;351(1666):301–30.
- [38] James HM, Guth E. J Chem Phys 1943;11(10):455–81.
- [39] Mullins L. Rubber Chem Technol 1948;21(2):281–300.
- [40] James HM, Guth E. J Chem Phys 1943;11(11):531.
- [41] Wang MC, Guth E. J Chem Phys 1952;20(7):1144–57.
- [42] De Gennes P-G. Scaling concepts in polymer physics. Cornell University Press; 1979.
- [43] Li F, Lu Y, Liu L, Zhang L, Dai J, Ma J. Polymer 2013;54(8):2158–65.
- [44] Grosch K, Harwood J, Payne A. Rubber Chem Technol 1968;41(5):1157–67.
- [45] Harwood J, Payne A. J Appl Polym Sci 1968;12(4):889–901.
- [46] Harwood J, Payne A, Whittaker R. J Macromol Sci Part B Phys 1971;5(2):473–86.
- [47] Mullins L, Tobin NR. J Appl Polym Sci 1965;9(9):2993.
- [48] Harwood JAC, Mullins L, Payne AR. J Appl Polym Sci 1965;9(9):3011.
- [49] Harwood JAC, Mullins L, Payne AR. J Polym Sci Part B-Polym Lett 1965;3(2pb):119.
- [50] Bueche F. J Appl Polym Sci 1960;4(10):107–14.
- [51] Bueche F. J Appl Polym Sci 1961;5(15):271–81.
- [52] Diaz R, Diani J, and Gilormini P. Polymer (DOI: <http://dx.doi.org/10.1016/j.polymer.2014.08.020>).
- [53] Meissner B, Matejka L. Polymer 2000;41(21):7749–60.
- [54] Meissner B. Polymer 2000;41(21):7827–41.
- [55] Sakulkaew K, Thomas AG, Busfield JJC. Polym Test 2011;30(2):163–72.
- [56] Kraus G. Reinforcement of elastomers. New York: Interscience; 1965.
- [57] Greensmith HW, Thomas AG. J Polym Sci 1955;18(88):189–200.